ACS APPLIED MATERIALS & INTERFACES

Research Article

www.acsami.org

Highly Stretchable and Wearable Graphene Strain Sensors with Controllable Sensitivity for Human Motion Monitoring

Jung Jin Park,[†,▽] Woo Jin Hyun,[‡,▽] Sung Cik Mun,[†] Yong Tae Park,[§] and O Ok Park*[,†]

[†]Department of Chemical and Biomolecular Engineering (BK21+ Graduate Program), Korea Advanced Institute of Science and Technology (KAIST), 291 Daehak-ro, Yuseong-gu, Daejeon 305-701, Republic of Korea

[‡]Department of Chemical Engineering and Materials Science, University of Minnesota, 421 Washington Avenue S.E., Minneapolis, Minnesota 55455, United States

[§]Department of Mechanical Engineering, Myongji University, 116 Myongji-ro, Cheoin-gu, Youngin, Gyeonggi-do 449-728, Republic of Korea

Supporting Information

ABSTRACT: Because of their outstanding electrical and mechanical properties, graphene strain sensors have attracted extensive attention for electronic applications in virtual reality, robotics, medical diagnostics, and healthcare. Although several strain sensors based on graphene have been reported, the stretchability and sensitivity of these sensors remain limited, and also there is a pressing need to develop a practical fabrication process. This paper reports the fabrication and characterization of new types of graphene strain sensors based on stretchable yarns. Highly stretchable, sensitive, and wearable sensors are realized by a layer-by-layer assembly method that is simple, low-cost, scalable, and solution-processable. Because of the yarn structures, these sensors exhibit high stretchability (up to 150%) and versatility, and can detect both large- and small-scale human motions. For this study, wearable electronics are fabricated with implanted sensors that can monitor diverse human motions, including joint movement, phonation, swallowing, and breathing.

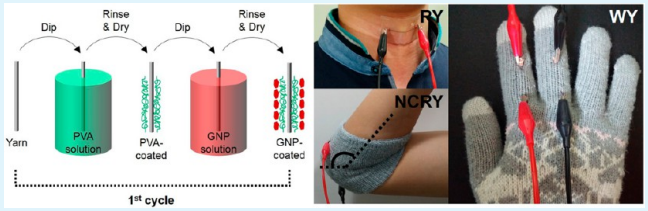

KEYWORDS: *stretchable electronics, strain sensor, graphene, layer-by-layer assembly, human motion monitoring*

1. INTRODUCTION

Strain sensors for monitoring human body motions have attracted considerable attention for developing diagnosis- and other healthcare-related electronic applications capable of interacting with the human body.[1−10] Monitoring human body motions can be classified into two categories: detection of large-scale motions (e.g., bending movements of the hands, arms, and legs) and detection of small-scale motions (e.g., subtle movements in the chest and neck during breathing, swallowing, and speaking). Sensors used for these two categories must have good stretchability for high strain and high sensitivity to small strain, respectively.[6−10] However, conventional strain sensors, which are based on metals and semiconductors, have limited stretchability and sensitivity;[6,7,10−12] therefore, they are incompatible with the human body. As such, there is increased demand for highly stretchable, sensitive, and wearable strain sensors for monitoring human body motions.[1−11]

Various approaches have been proposed to meet this demand through the use of nanomaterials such as nanoparticles,[1,2,13] nanowires,[11] carbon nanotubes (CNT),[3,4,6,14,15] and graphene.[7−10,15−23] In particular, graphene, a two-dimensional hexagonally structured material, consisting of sp^2-bonded carbon atoms,[20,22,24] has been used extensively for strain sensors, because of its outstanding electrical and mechanical properties.[8−10,20−26] Several studies have been conducted on strain sensors based on graphene prepared by chemical vapor deposition (CVD).[9,16−23] CVD-grown few-layer graphene is highly sensitive and enables detection of small-scale motions of the human body.[9,20,23] Highly stretchable CVD-grown graphene, with three-dimensional (3D) macroporous structures,[22] has also been reported to overcome the limited stretchability (up to 7%) of the CVD-grown graphene films.[17−20] However, CVD-grown graphene sensors are fabricated through an expensive and complicated process that is unsuitable for practical applications. To address this issue, highly stretchable strain sensors have recently been developed by a vacuum filtration process with a reduced graphene oxide dispersion.[10] This approach produces highly stretchable (up to 100%) sensors for the detection of large-scale human body motions. However, controlling the sensitivity of the sensor for measuring diverse human body motions remains challenging. Therefore, the challenge lies in developing, by means of an inexpensive and scalable process, a graphene strain sensor that has appropriate stretchability and sensitivity for monitoring human body motions.

Received: January 22, 2015
Accepted: March 4, 2015
Published: March 4, 2015

DOI: 10.1021/acsami.5b00695
ACS Appl. Mater. Interfaces 2015, 7, 6317−6324

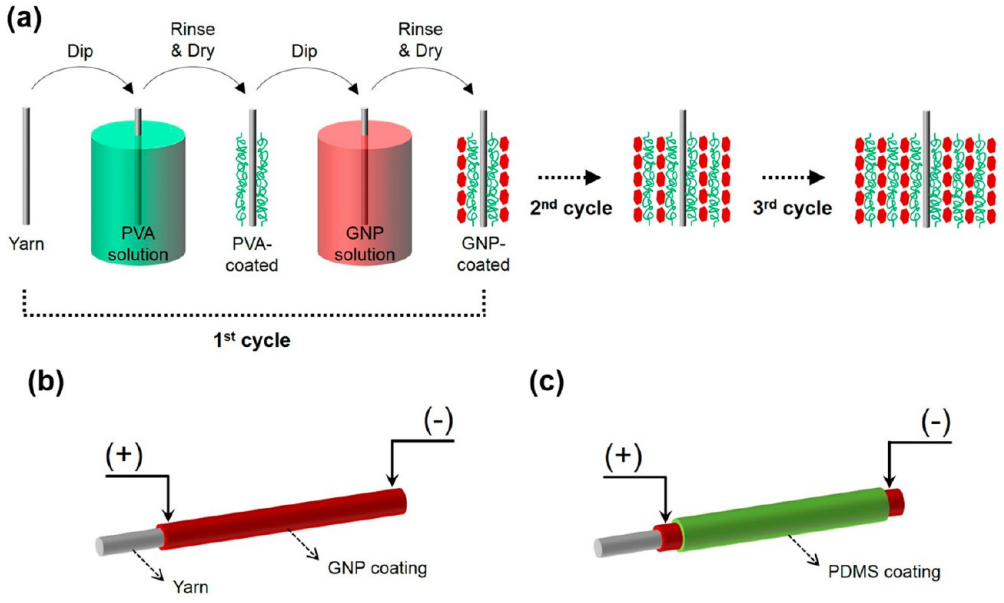

Figure 1. (a) Steps in the LbL process for fabrication of a graphene strain sensor using a stretchable yarn. Each cycle of the process includes one PVA and one GNP coating. The thickness of the GNP layer can be increased by repeating the LbL cycle. After repetition of a number (n) of PVA and GNP coatings, n layers of PVA and GNP were coated alternatively on the surface of the yarn. Schematic illustrations of the graphene strain sensors based on stretchable yarns (b) without and (c) with PDMS coating.

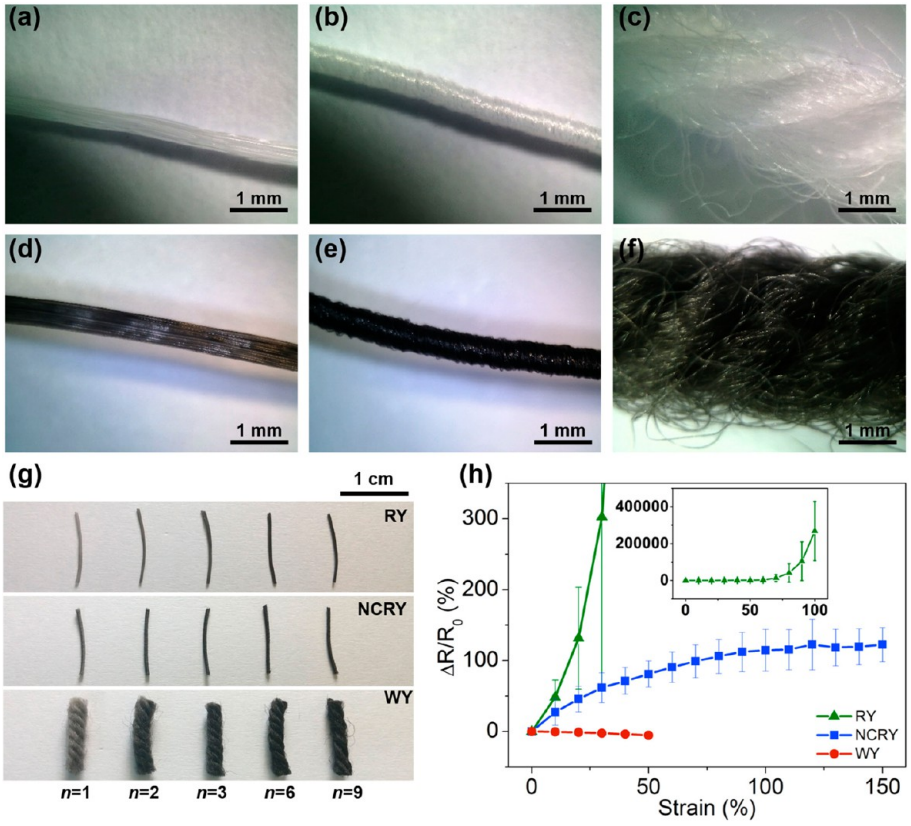

Figure 2. Photographs of RY, NCRY, and WY, (a, b, c) before and (d, e, f) after three cycles of the LbL process. (g) Comparison of the stretchable yarns for varying number (n) of LbL cycles. (h) Relative resistance change of the three graphene strain sensors as a function of the applied strain. (Inset in panel (h) shows a large-scale plot for the RY sensor.)

In this work, we develop highly stretchable, sensitive, and wearable graphene strain sensors that are based on a dispersion of graphene nanoplatelets (GNP) and stretchable yarns as frameworks. The graphene strain sensors were prepared by a layer-by-layer (LbL) assembly technique that is a simple, low-cost, scalable, and solution-processable method for producing thin-film coatings of controllable thickness.[27−36] Three types of strain sensors, made from different commercialized yarns, were

DOI: 10.1021/acsami.5b00695
ACS Appl. Mater. Interfaces 2015, 7, 6317−6324

fabricated in order to investigate the effect of the yarn structure on the piezoresistive properties. Depending on the yarn structures, these sensors exhibited high stretchability (up to 150%), controllable sensitivity, and high versatility, which enabled their use in detecting large- and small-scale human body motions. Moreover, since fabrics can be easily sewn with the yarns, this approach enables easy application of the sensors to diverse human body parts. To demonstrate the feasibility of this approach, several wearable applications were fabricated using the graphene strain sensors and their performance was characterized.

2. RESULTS AND DISCUSSION

Figure 1 schematically depicts the fabrication of graphene strain sensors carried out through repetition of poly(vinyl alcohol) (PVA) and GNP coatings (see Experimental Section for details) using the LbL assembly technique. The yarn was coated with PVA by first immersing in a PVA solution, rinsing with deionized (DI) water, and drying with air. The PVA was then attached to the surface of the yarn by noncovalent bonding interactions, including hydrogen bonding, van der Waals, and hydrophobic attraction.[29−31,37,38] The yarn was subsequently dipped in a GNP solution, rinsed with DI water, and dried with air, in order to deposit graphene on the PVA layer. Poly(4-styrenesulfonic acid) (PSS) was added to the GNP solution to facilitate stable dispersion of the GNP in DI water. This addition was necessary because aromatic rings of PSS adsorb to the graphene surface, because of hydrophobic and $\pi-\pi$ interactions, and hydrophilic sulfonic groups of PSS prevent the agglomeration of hydrophobic graphene in polar solvents such as water.[31,32,39] The sulfonic groups ($-SO_3H$) of PSS also contribute to the formation of hydrogen bonds with the hydroxyl groups ($-OH$) of PVA.[31,33,40] In addition, van der Waals, charge transfer, and hydrophobic interactions contribute to the binding of PVA to GNP with PSS.[29−36] After the repetition of a number (n) of cycles, the yarn was alternatively coated by n layers of PVA and GNP.

The structural effect of the yarn on the piezoresistive property of the strain sensor was investigated by comparing the sensors made from three types of stretchable yarns, namely, rubber (RY), nylon covered rubber (NCRY), and wool yarns (WY) (see Figure S1 in the Supporting Information). RY (thickness of ∼0.45 mm) consists of thin and straight rubber fibers. NCRY (thickness of ∼0.55 mm) consists of a bunch of rubber fibers surrounded by helical nylon fibers. WY (thickness of ∼3 mm) is made with crimped and twisted wool fibers. Comparison of the bare yarns to those after LbL assembly processing (three cycles) reveals that the white yarns became black (Figure 2a−f), because of the GNP layer. Figure 2g shows that the black yarn became darker as the number of LbL cycles increases, indicative of an increase in the thickness of the GNP layer. Furthermore, all three types of yarns retained good stretchability (see Figure S2a in the Supporting Information), even after undergoing GNP LbL coating.

The graphene strain sensors (Figure 1b) made by using GNP-coated yarns were characterized with regard to the applied strain. Figure 2h shows the relative resistance change of the sensors after three LbL cycles, as a function of the applied strain. The relative resistance change ($\Delta R/R_0$) is defined as the ratio of the resistance change (ΔR) to the resistance (R_0) at the initial state. The sensors exhibited different piezoresistive responses to the strain; i.e., with increasing strain, the resistance of the RY and NCRY sensors increased, while that of the WY sensor decreased. In particular, the resistance of the RY sensor increased significantly, compared to that of the NCRY sensor. These piezoresistive responses originate from the different deformation behaviors of the yarns during stretching (see Figure S3 in the Supporting Information). Figure 3 shows

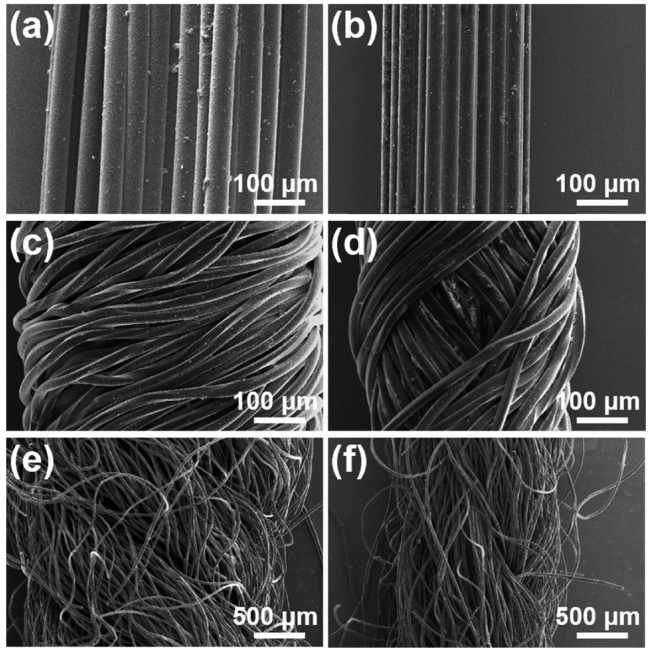

Figure 3. SEM images of the graphene strain sensors based on RY, NCRY, and WY, (a, c, e) without and (b, d, f) with strain (100%, 100%, and 50%, respectively).

detailed SEM images of the yarn structures of the graphene strain sensors without and with the strain. The bunch of straight rubber fibers (Figure 3a) that comprise the RY become elongated when stretched (Figure 3b). This stretching resulted in the generation of cracks (Figure 4a) in the GNP coating on the surface of the fibers, which led to the breakage of electrical paths and, hence, a significant increase in electrical resistance. On the other hand, since NCRY consists of inner rubber and outer nylon fibers, which surround the rubber fibers in a spiral (Figure 3c), PVA and GNP were mainly adsorbed onto the outer fibers, while the inner fibers are partially coated during the LbL process (see Figure S4 in the Supporting Information). Hence, the piezoresistive property of the NCRY sensor depends mainly on the deformation of the outer nylon fibers. Under strain, the inner rubber fibers were stretched in the direction of the external force, while the nylon fibers were not directly stretched but deformed along the stretching direction (see Figure 3d). This dual structure minimized the elongation of the nylon fibers and suppressed the formation of prominent cracks in the GNP coating (Figure 4b), which resulted in a smaller increase in the resistance of the NCRY sensor, compared to that of the RY sensor for the same strain. The gauge factor $[(\Delta R/R_0)/(\varepsilon)]$ of the sensors (see Figure S5a in the Supporting Information), where ε is the applied strain, was calculated in order to determine the sensitivity of the sensor to strain. The gauge factor of the RY sensor increased exponentially with increasing strain and was much higher than that of the NCRY sensor. This implies that the graphene coating on the former is much more sensitive to the strain than that of the latter. Moreover, Figure 2h shows that, in contrast to

DOI: 10.1021/acsami.5b00695
ACS Appl. Mater. Interfaces 2015, 7, 6317−6324

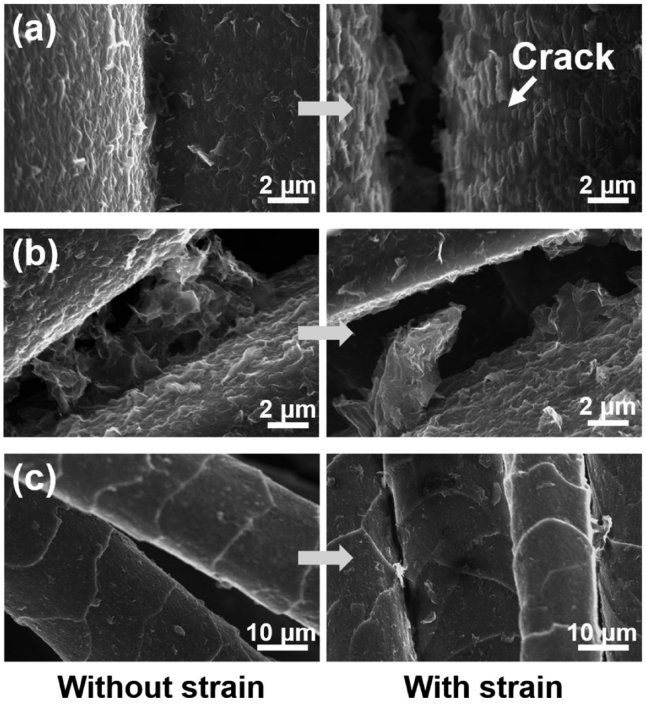

Figure 4. High-magnification SEM images of the graphene strain sensors based on (a) RY, (b) NCRY, and (c) WY, without and with strain (100%, 100%, and 50%, respectively).

the RY and NCRY sensors, the resistance of the WY sensor decreased with increasing strain. This piezoresistive behavior is different from that of conventional graphene strain sensors, whose resistances increase with increasing strain.[7−10,17−23] The unique piezoresistive property of the WY sensor can be attributed to its yarn structure that is composed of crimped and twisted fine wool fibers (see Figure 3e). When WY was stretched, the curled wool fibers became straightened and closer to each other (Figure 3f and 4c). Furthermore, the subsequent contact between the GNP-coated wool fibers resulted in an increase in electrical paths and, hence, a decrease in the electrical resistance.

When strained, RY, NCRY, and WY sensors were capable of stretching up to 100%, 150%, and 50%, respectively. As shown in Figure 1c, as well as in Figure S2b in the Supporting Information, the RY and NCRY sensors were coated with polydimethylsiloxane (PDMS) in order to avoid possible delamination of the GNP coating from the surfaces due to high strain. The WY sensor was not coated because WY loses its good stretchability and unique electrical property after coating with PDMS. In addition, the WY sensor did not exhibit any significant delamination of the GNP coating for strains below 50%. However, when WY was stretched above 50% strain, wool fibers were damaged and not recovered, leading to the permanent deformation and the increase in resistance of the WY sensor. Figure 5a shows the relative resistance change for the PDMS-coated graphene strain sensors. The RY sensor maintained an overall high sensitivity, even after being coated, but $\Delta R/R_0$ decreased (see inset in Figure 5a) with high strain (≥70%), compared to that of the sensors without the PDMS coating (inset of Figure 2h). This decrease results because the coating prevented delamination of the GNP layer, thereby suppressing unexpected degradation arising from delamination under high strain. Furthermore, the PDMS-coated NCRY sensor showed an excellent linear relationship (R^2 = 0.98; this is the coefficient of determination for the linear regression) between the relative resistance change and the applied strain, and the almost-constant gauge factor (see Figure S5b in the

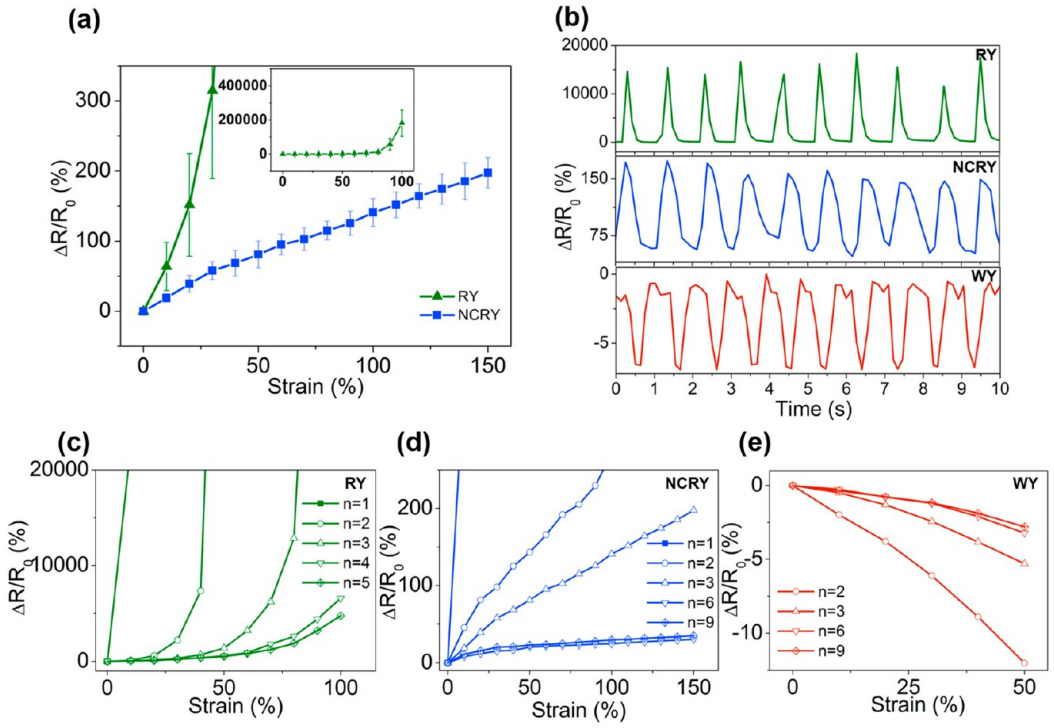

Figure 5. (a) Relative resistance change of the RY and NCRY sensors with PDMS coating. (b) Response curves of the RY, NCRY, and WY sensors for repetition of strain (~80%, ~100%, and ~40%, respectively) at a frequency of 1 Hz. Also shown is the relative resistance change of the graphene strain sensors using (c) RY, (d) NCRY, and (e) WY for a varying number (n) of LbL cycles.

DOI: 10.1021/acsami.5b00695
ACS Appl. Mater. Interfaces 2015, 7, 6317−6324

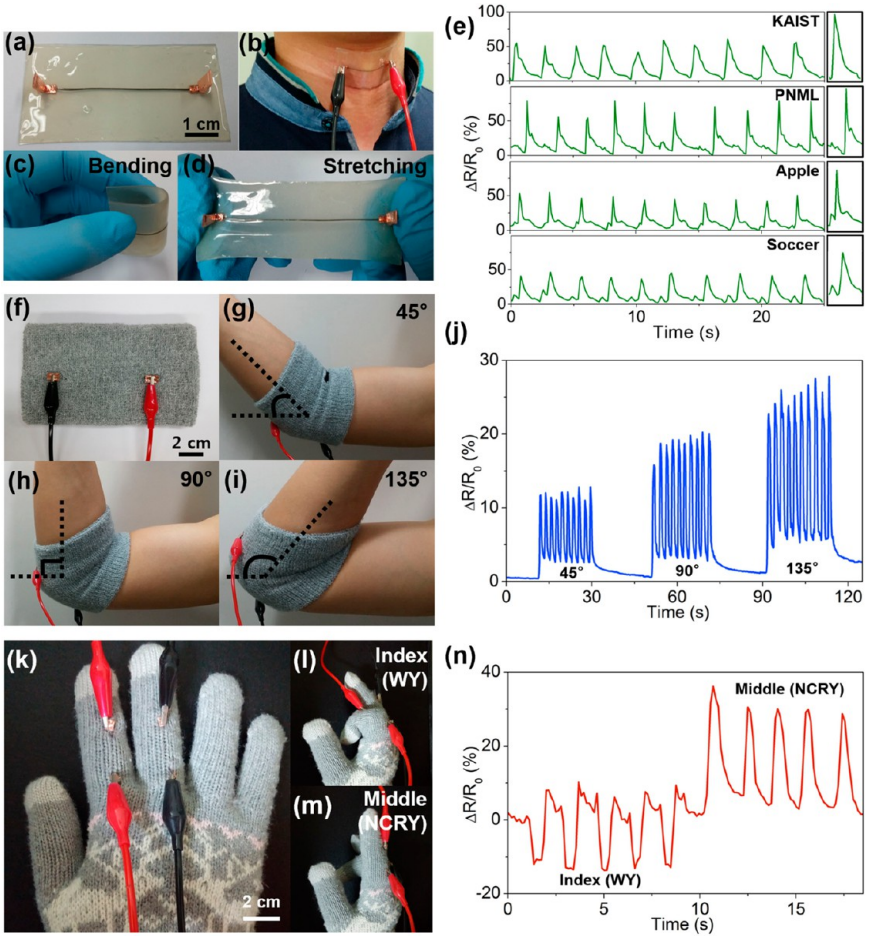

Figure 6. (a–d) Photographs showing the RY strain sensor embedded in an elastomeric patch that is bendable and stretchable, for detection of the small-scale motions of the throat. (e) Relative resistance change of the RY strain sensor associated with muscle motions for different phonations. (f–i) Photographs showing theNCRY strain sensor sewed in an elbow wrap to monitor the bending motion of the arm at different angles of 45°, 90°, and 135°. (j) Relative resistance change for the NCRY strain sensor according to the bending motions. (k–m) Photographs showing the WY and NCRY sensors implanted in a glove for recording the movements of the index and middle fingers. (n) Relative resistance change of the sensors, showing distinct signals.

Supporting Information) with increasing strain. This suggests that the negative structural effect on the electrical property was eliminated by the PDMS coating, and that the NCRY sensor was mainly affected by the deformation of the GNP layers coated on the nylon fibers. In addition, the PDMS coating is favorable for RY and NCRY sensors, both in terms of reproducibility and durability. Therefore, further experiments were conducted using PDMS-coated RY and NCRY sensors. Figure 5b shows the response curves of each sensor, during a repetition of applying strain and releasing at a frequency of ~1 Hz. All three types of graphene strain sensors exhibited a reversible piezoresistive property, a fast response, and good reproducibility of signals. Moreover, the sensitivity of the sensors could be tuned by controlling the number of LbL cycles. Figures 5c–e show the relative resistance change of each sensor at different numbers of LbL cycles. The value of $\Delta R/R_0$ decreased as the number of LbL cycles increased, indicating that the sensitivity of the sensors increases as the thickness of the GNP coatings decreases. The piezoresistivity of the sensors with GNP was mainly dependent on the overlap area and contact resistance.[7,8] Hence, the sensors with the large thickness of LbL film exhibited low sensitivity, because the overlap area among adjacent GNPs increased with an increment of the thickness of GNP coating, which suppressed the breakage of electrical paths under strain (see Figure S6 in the Supporting Information).[7,8] Although their sensitivities changed, the sensors still exhibited unique characteristics (i.e., high sensitivity of RY sensors, high stretchability (up to 150%) and linear piezoresistivity behavior of NCRY sensors, and the unconventional piezoresistive property of WY sensors). The diversity of motions measured by these sensors, as well as their stretchability and sensitivity, were also superior to those of previously studied graphene strain sensors (see Table S1 in the Supporting Information).

The graphene strain sensors can be used for wearable applications, because the stretchable yarns can be easily implanted in general items. Diverse motions in different human body parts, correlated to the piezoresistive characteristics of each sensor, were monitored by several wearable sensors made of the three GNP-coated yarns. The high sensitivity of the RY sensor is desirable for the detection of small-scale human motion such as delicate movements of the throat. The RY sensor was embedded in the PDMS layer on an elastomeric medical patch (Figure 6a), and the patch was attached to the throat (Figure 6b). Since the elastomeric patch can be easily bent and stretched (see Figures 6c and 6d), it was able to deliver the motions of the throat to the strain sensor. When the tester spoke several words, including "KAIST",

DOI: 10.1021/acsami.5b00695
ACS Appl. Mater. Interfaces 2015, 7, 6317–6324

"PNML", "apple", and "soccer", the sensor recorded specific patterns (Figure 6e) regarding the value of $\Delta R/R_0$ for each phonation, since each word resulted in distinct movements of the laryngeal prominence. The same patterns were produced when the words were repeated, which represents a good possibility for use as acoustic sensors with excellent reliability. The RY sensor in the patch could also monitor swallowing by detecting the movement of the Adam's apple (see Figure S7a in the Supporting Information). Furthermore, when attached to the chest, it could record each breathing cycle—the combination of one inhalation and one exhalation, which made the sensor stretch and release, respectively (see Figure S7b in the Supporting Information). In contrast to the RY sensor, the NCRY sensor satisfies the requirements for large-scale motions and accurate detections, because of its high stretchability and linear piezoresistivity behavior. To monitor elbow bending, an elbow wrap was sewn with the NCRY sensor (Figure 6f), which was then placed into the arm so that the sensor is located at the outside of the elbow. When the tester bent his arm with angles of 45°, 90°, and 135° (see Figures 6g, 6h, and 6i, respectively), the NCRY sensor produced signals (Figure 6j) with different intensities since larger bending motions resulted in greater elongations of the sensor. The proportional increase in the relative resistance change with increasing bending angle means that the sensor has the ability to both detect and quantify the applied strain. When the NCRY sensor was applied to the wrist, its bending motion could be also easily monitored (view Movie S1 in the Supporting Information). A data glove was also made with the WY and NCRY sensors, in order to compare their piezoresistive response to the bending motions of the fingers. The index and middle fingers of the glove (Figure 6k) were sewn with the WY and NCRY sensors, respectively, and the sensors were placed outside of the finger joints. Individual bending of the index (Figure 6l) and middle (Figure 6m) fingers resulted in opposite sensing signals (see Figure 6n and Movie S2 in the Supporting Information); the resistance of the WY and NCRY sensors decreased and increased, respectively, under strain. When two sensors operate simultaneously to detect different parts of the body, these opposite responses to similar bending motions can be advantageous for identifying the sensor that produces the signal.

3. CONCLUSION

In summary, three types of graphene strain sensors, based on stretchable yarns, were fabricated from a GNP dispersion and a PVA solution using the LbL assembly technique, which is facile, cost-effective, scalable, and solution-processable. The sensors were characterized by their piezoresistive responses, which are dependent on the yarn structure; these responses enabled the sensors to monitor diverse human body motions. The highly sensitive RY sensor was capable of detecting small-scale motions in the throat and the chest. The NCRY sensor precisely detected large-scale motion, such as the bending movements of the arm and hand, because of high stretchability (up to 150%), and good linear relationship between the strain and the relative resistance change. In contrast, WY sensors exhibited a negative sensing response that is distinct from that of conventional strain sensors. Therefore, these sensors enable easy identification of the body part that moves. The aforementioned findings confirm that this study provides a practical and meaningful approach of realizing graphene strain sensors for monitoring motions of the human body.

4. EXPERIMENTAL SECTION

Preparation of Graphene Dispersion and PVA Solution. Graphene nanoplatelets (GNP) (No. N002-PDR, $XY < 10\ \mu m$, $Z \approx 1$ nm) provided by Angstron Materials, were prepared by chemical exfoliation and thermal reduction. Poly(4-styrenesulfonic acid) (PSS) ($M_w \approx 75\,000$) and poly(vinyl alcohol) (PVA) ($M_w \approx 89\,000$–$98\,000$) were purchased from Sigma–Aldrich. The graphene dispersion was obtained by adding GNP (0.1 wt %) and PSS (0.1 wt %) to deionized (DI) water, followed by ultrasonication for 3 h. Similarly, the PVA solution was obtained by stirring PVA into DI water for 10 min at 80 °C, followed by sonication for 30 min.

Fabrication of the Graphene Strain Sensors. Yarns were immersed in the PVA solution for 5 min, rinsed in DI water, and dried in air. PVA was used as the precursor and counterpart layers to form the stable and robust GNP coating. They were then submerged in the graphene dispersion for 5 min, followed by rinsing and drying. The two steps were repeated in order to control the thickness of the GNP layer deposited on the yarns. The PDMS coatings were prepared by first degassing the mixture of the PDMS base and the curing agent (No. SH9555, Dow Corning Toray) (15:1 weight ratio) in a vacuum desiccator for 15 min. The graphene-coated yarns then were dipped in the degassed mixture and kept in a vacuum desiccator for 10 min to in order to remove the bubbles between the yarns and the PDMS. The graphene-coated yarns were subsequently removed from the PDMS mixture and cured at 65 °C for 45 min.

Characterization. The graphene strain sensors were observed via field-emission scanning electron microscopy (FE-SEM) (Model Sirion, FEI) and an optical microscope (Model B008, Ecwox). The electric properties were measured by using a source meter (Model 2400, Keithley). In addition, silver paste (No. P-100, ELCOAT) and copper conductive tape (3M) were used for better contact between the source meter and the graphene-coated yarns.

■ ASSOCIATED CONTENT

Ⓢ Supporting Information

Supporting Information has been provided on the following topics: SEM images of pristine yarns; photographs of the graphene strain sensors with and without PDMS coating; schematic drawing for comparison of yarn structures; photographs of untangled NCRY without and with GNP coating; gauge factor versus strain curves of graphene strain sensors; and relative resistance changes of the RY sensor attached to human body. This material is available free of charge via the Internet at http://pubs.acs.org.

■ AUTHOR INFORMATION

Corresponding Author

*E-mail: oopark@kaist.ac.kr.

Author Contributions

[▽]These authors contributed equally to this work.

Author Contributions

The manuscript was written through contributions of all authors. All authors have given approval to the final version of the manuscript.

Notes

The authors declare no competing financial interest.

■ ACKNOWLEDGMENTS

This research was supported by a grant (No. 10037689) from the Fundamental R&D Program for Technology of World Premier Materials (WPM) funded by the Ministry of Trade, Industry, and Energy (MOTIE, Korea). The authors thank J. M. Do in SnM for technical assistance with the electrical property measurement.

DOI: 10.1021/acsami.5b00695
ACS Appl. Mater. Interfaces 2015, 7, 6317–6324

REFERENCES

(1) Segev-Bar, M.; Haick, H. Flexible Sensors Based on Nanoparticles. *ACS Nano* **2013**, *7*, 8366−8378.

(2) Son, D.; Lee, J.; Qiao, S.; Ghaffari, R.; Kim, J.; Lee, J. E.; Song, C.; Kim, S. J.; Lee, D. J.; Jun, S. W.; Yang, S.; Park, M.; Shin, J.; Do, K.; Lee, M.; Kang, K.; Hwang, C. S.; Lu, N.; Hyeon, T.; Kim, D.-H. Multifunctional Wearable Devices for Diagnosis and Therapy of Movement Disorders. *Nat. Nanotechnol.* **2014**, *9*, 397−404.

(3) Park, S.; Vosguerichian, M.; Bao, Z. A Review of Fabrication and Applications of Carbon Nanotube Film-Based Flexible Electronics. *Nanoscale* **2013**, *5*, 1727−1752.

(4) Jung, S.; Kim, J. H.; Kim, J.; Choi, S.; Lee, J.; Park, I.; Hyeon, T.; Kim, D.-H. Reverse-Micelle-Induced Porous Pressure-Sensitive Rubber for Wearable Human Machine Interfaces. *Adv. Mater.* **2014**, *26*, 4825−4830.

(5) Pang, C.; Koo, J. H.; Nguyen, A.; Caves, J. M.; Kim, M.-G.; Chortos, A.; Kim, K.; Wang, P. J.; Tok, J. B.-H.; Bao, Z. Highly Skin-Conformal Microhairy Sensor for Pulse Signal Amplification. *Adv. Mater.* **2015**, *27*, 634−640.

(6) Yamada, T.; Hayamizu, Y.; Yamamoto, Y.; Yomogida, Y.; Izadi-Najafabadi, A.; Futaba, D. N.; Hata, K. A Stretchable Carbon Nanotube Strain Sensor for Human-Motion Detection. *Nat. Nanotechnol.* **2011**, *6*, 296−301.

(7) Hempel, M.; Nezich, D.; Kong, J.; Hofmann, M. A Novel Class of Strain Gauges Based on Layered Percolative Films of 2D Materials. *Nano Lett.* **2012**, *12*, 5714−5718.

(8) Tian, H.; Shu, Y.; Cui, Y.-L.; Mi, W.-T.; Yang, Y.; Xie, D.; Ren, T.-L. Scalable Fabrication of High-Performance and Flexible Graphene Strain Sensors. *Nanoscale* **2014**, *6*, 699−705.

(9) Wang, Y.; Wang, L.; Yang, T.; Li, X.; Zang, X.; Zhu, M.; Wang, K.; Wu, D.; Zhu, H. Wearable and Highly Sensitive Graphene Strain Sensors for Human Motion Monitoring. *Adv. Funct. Mater.* **2014**, *24*, 4666−4670.

(10) Yan, C.; Wang, J.; Kang, W.; Cui, M.; Wang, X.; Foo, C. Y.; Chee, K. J.; Lee, P. S. Highly Stretchable Piezoresistive Graphene−Nanocellulose Nanopaper for Strain Sensors. *Adv. Mater.* **2014**, *26*, 2022−2027.

(11) Amjadi, M.; Pichitpajongkit, A.; Lee, S.; Ryu, S.; Park, I. Highly Stretchable and Sensitive Strain Sensor Based on Silver Nanowire−Elastomer Nanocomposite. *ACS Nano* **2014**, *8*, 5154−5163.

(12) Barlian, A. A.; Park, W.-T.; Mallon, J. R.; Rastegar, A. J.; Pruitt, B. L. Review: Semiconductor Piezoresistance for Microsystems. *Proc. IEEE* **2009**, *97*, 513−552.

(13) Radha, B.; Sagade, A. A.; Kulkarni, G. U. Flexible and Semitransparent Strain Sensors Based on Micromolded Pd Nanoparticle-Carbon μ-Stripes. *ACS Appl. Mater. Interfaces* **2011**, *3*, 2173−2178.

(14) Lipomi, D. J.; Vosgueritchian, M.; Tee, B. C-K.; Hellstrom, S. L.; Lee, J. A.; Fox, C. H.; Bao, Z. Skin-Like Pressure and Strain Sensors Based on Transparent Elastic Films of Carbon Nanotubes. *Nat. Nanotechnol.* **2011**, *6*, 788−792.

(15) Luo, S.; Liu, T. SWCNT/Graphite Nanoplatelet Hybrid Thin Films for Self-Temperature-Compensated, Highly Sensitive, and Extensible Piezoresistive Sensors. *Adv. Mater.* **2013**, *25*, 5650−5657.

(16) Xu, R.; Lu, Y.; Jiang, C.; Chen, J.; Mao, P.; Gao, G.; Zhang, L.; Wu, S. Facile Fabrication of Three-Dimensional Graphene Foam/Poly(dimethylsiloxane) Composites and Their Potential Application as strain sensor. *ACS Appl. Mater. Interfaces* **2014**, *6*, 13455−13460.

(17) Zhao, J.; He, C.; Yang, R.; Shi, Z.; Cheng, M.; Yang, W.; Xie, G.; Wang, D.; Shi, D.; Zhang, G. Ultra-Sensitive Strain Sensors Based on Piezoresistive Nanographene Films. *Appl. Phys. Lett.* **2012**, *101*, 063112.

(18) Lee, Y.; Bae, S.; Jang, H.; Jang, S.; Zhu, S.-E.; Sim, S. H.; Song, Y. I.; Hong, B. H.; Ahn, J.-H. Wafer-Scale Synthesis and Transfer of Graphene Films. *Nano Lett.* **2010**, *10*, 490−493.

(19) Fu, X.-W.; Liao, Z.-M.; Zhou, J.-X.; Zhou, Y.-B.; Wu, H.-C.; Zhang, R.; Jing, G.; Xu, J.; Wu, X.; Guo, W.; Yu, D. Strain Dependent Resistance in Chemical Vapor Deposition Grown Graphene. *Appl. Phys. Lett.* **2011**, *99*, 213107.

(20) Bae, S.-H.; Lee, Y.; Sharma, B. K.; Lee, H.-J.; Kim, J.-H.; Ahn, J.-H. Graphene-Based Transparent Strain Sensor. *Carbon* **2013**, *51*, 236−242.

(21) Li, X.; Zhang, R.; Yu, W.; Wang, K.; Wei, J.; Wu, D.; Cao, A.; Li, Z.; Cheng, Y.; Zheng, Q.; Ruoff, R. S.; Zhu, H. Stretchable and Highly Sensitive Graphene-on-Polymer Strain Sensors. *Sci. Rep.* **2012**, *2*, 870.

(22) Chen, Z.; Ren, W.; Gao, L.; Liu, B.; Pei, S.; Cheng, H.-M. Three-Dimensional Flexible and Conductive Interconnected Graphene Networks Grown by Chemical Vapour Deposition. *Nat. Mater.* **2011**, *10*, 424−428.

(23) Wang, Y.; Yang, T.; Lao, J.; Zhung, R.; Zhang, Y.; Zhu, M.; Li, X.; Zang, X.; Wang, K.; Jin, H.; Wang, L.; Zhu, H. Ultra-sensitive graphene strain sensor for sound signal acquisition and recognition. *Nano Res.* **2015**, DOI: 10.1007/s12274-014-0652-3.

(24) Rao, C. N. R.; Sood, A. K.; Subrahmanyam, K. S.; Govindaraj, A. Graphene: The New Two-Dimensional Nanomaterial. *Angew. Chem., Int. Ed.* **2009**, *48*, 7752−7777.

(25) Hyun, W. J.; Park, O. O.; Chin, B. D. Foldable Graphene Electronic Circuits Based on Paper Substrates. *Adv. Mater.* **2013**, *25*, 4729−4734.

(26) Park, Y. T.; Qian, Y.; Chan, C.; Suh, T.; Nejhad, M. G.; Macosko, C. W.; Stein, A. Epoxy Toughening with Low Graphene Loading. *Adv. Funct. Mater.* **2015**, *25*, 575−585.

(27) Park, Y. T.; Ham, A. Y.; Grunlan, J. C. High Electrical Conductivity and Transparency in Deoxycholate-Stabilized Carbon Nanotube Thin Films. *J. Phys. Chem. C* **2010**, *114*, 6325−6333.

(28) Park, Y. T.; Ham, A. Y.; Grunlan, J. C. Heating and Acid Doping Thin Film Carbon Nanotube Assemblies for High Transparency and Low Sheet Resistance. *J. Mater. Chem.* **2011**, *21*, 363−368.

(29) Serizawa, T.; Kamimura, S.; Kawanishi, N.; Akashi, M. Layer-by-Layer Assembly of Poly(vinyl alcohol) and Hydrophobic Polymers Based on Their Physical Adsorption on Surfaces. *Langmuir* **2002**, *18*, 8381−8385.

(30) K, J.; Hsu, S. L.; McCarthy, T. J. Versatile multilayer thin film preparation using hydrophobic interactions, crystallization, and chemical modification of poly(vinyl alcohol). *Langmuir* **2007**, *23*, 3260−3264.

(31) Shim, B. S.; Tang, Z.; Morabito, M. P.; Agarwal, A.; Hong, H.; Kotov, N. A. Integration of Conductivity, Transparency, and Mechanical Strength into Highly Homogeneous Layer-by-Layer Composites of Single-Walled Carbon Nanotubes for Optoelectronics. *Chem. Mater.* **2007**, *19*, 5467−5474.

(32) Li, Z.; Wang, J.; Liu, X.; Liu, S.; Ou, J.; Yang, S. Electrostatic Layer-by-Layer Self-Assembly Multilayer Films Based on Graphene and Manganese Dioxide Sheets as Novel Electrode Materials for Supercapacitors. *J. Mater. Chem.* **2011**, *21*, 3397−3403.

(33) Lee, H.; Mensire, R.; Cohen, R. E.; Rubner, M. F. Strategies for Hydrogen Bonding Based Layer-by-Layer Assembly of Poly(vinyl alcohol) with Weak Polyacids. *Macromolecules* **2012**, *45*, 347−355.

(34) Zhu, J.; Zhang, H.; Kotov, N. A. Thermodynamic and Structural Insights into Nanocomposites Engineering by Comparing Two Materials Assembly Techniques for Graphene. *ACS Nano* **2013**, *7*, 4818−4829.

(35) Jhu, J.; Shim, B. S.; Prima, M. D.; Kotov, N. A. Transparent Conductors from Carbon Nanotubes LBL-assembled with Polymer Dopant with π-π Electron Transfer. *J. Am. Chem. Soc.* **2011**, *133*, 7450−7460.

(36) Shim, B. S.; Zhu, J.; Jan, E.; Critchley, K.; Ho, S.; Podsiadlo, P.; Sun, K.; Kotov, N. A. Multiparameter Structural Optimization of Single-Walled Carbon Nanotube Composites: Toward Record Strength, Stiffness, and Toughness. *ACS Nano* **2009**, *7*, 1711−1722.

(37) Wu, X.-Y.; Huang, S.-W.; Zhang, J.-T.; Zhuo, R.-X. Preparation and Characterization of Novel Physically Cross-Linked Hydrogels Composed of Poly(vinyl alcohol) and Amine-Terminated Polyamidoamine Dendrimer. *Macromol. Biosci.* **2004**, *4*, 71−75.

(38) Belanger, D.; Tong, X.; Soumare, S.; Dory, Y. L.; Zhao, Y. Cyclic Peptide-Polymer Complexes and Their Self-Assembly. *Chem.—Eur. J.* **2009**, *15*, 4428−4436.

DOI: 10.1021/acsami.5b00695
ACS Appl. Mater. Interfaces 2015, 7, 6317−6324

(39) Stankovich, S.; Piner, R. D.; Chen, X.; Wu, N.; Nguyen, S. T.; Ruoff, R. S. Stable Aqueous Dispersions of Graphitic Nanoplatelets via the Reduction of Exfoliated Graphite Oxide in the Presence of Poly(sodium 4-styrenesulfonate). *J. Mater. Chem.* **2006**, *16*, 155−158.
(40) Sahu, A. K.; Selvarani, G.; Bhat, S. D.; Pitchumani, S.; Sridhar, P.; Shukla, A. K.; Narayanan, N.; Banerjee, A.; Chandrakumar, N. Effect of Varying Poly(styrene sulfonic acid) Content in Poly(vinyl alcohol)−Poly(styrene sulfonic acid) Blend Membrane and Its Ramification in Hydrogen−Oxygen Polymer Electrolyte Fuel Cells. *J. Membr. Sci.* **2008**, *319*, 298−305.

DOI: 10.1021/acsami.5b00695
ACS Appl. Mater. Interfaces 2015, 7, 6317−6324